

## Collisional particle pressure measurements in solid–liquid flows

By R. ZENIT, M. L. HUNT AND C. E. BRENNEN

Division of Engineering and Applied Sciences, California Institute of Technology, Pasadena,  
CA 91125, USA

(Received 5 February 1997 and in revised form 29 August 1997)

Experiments were conducted to measure the collisional particle pressure in both cocurrent and countercurrent flows of liquid–solid mixtures. The collisional particle pressure, or granular pressure, is the additional pressure exerted on the containing walls of a particulate system due to the particle collisions. The present experiments involve both a liquid-fluidized bed using glass, plastic or steel spheres and a vertical gravity-driven flow using glass spheres. The particle pressure was measured using a high-frequency-response flush-mounted pressure transducer. Detailed recordings were made of many different particle collisions with the active face of this transducer. The solids fraction of the flowing mixtures was measured using an impedance volume fraction meter. Results show that the magnitude of the measured particle pressure increases from low concentrations (<10% solid volume fraction), reaches a maximum for intermediate values of solid fraction (30–40%), and decreases again for more concentrated mixtures (>40%). The measured collisional particle pressure appears to scale with the particle dynamic pressure based on the particle density and terminal velocity. Results were obtained and compared for a range of particle sizes, as well as for two different test section diameters.

In addition, a detailed analysis of the collisions was performed that included the probability density functions for the collision duration and collision impulse. Two distinct contributions to the collisional particle pressure were identified: one contribution from direct contact of particles with the pressure transducer, and the second one resulting from particle collisions in the bulk that are transmitted through the liquid to the pressure transducer.

---

### 1. Introduction

The particle pressure can be defined as the pressure exerted on the containing walls due to the presence of particles. Hence, it can be considered a measure of the momentum transport attributed to the motion of particles and their interactions.

In many theoretical models of multiphase flows, a separate set of equations is usually written for each of the phases, which are coupled through an interaction term. Pressures,  $P_f$  on the dispersed phase and  $P_p$  in the discrete phase, are defined and the corresponding pressure gradient terms are included in the momentum conservation equation. While  $\partial P_f / \partial x_i$  does not impose any conceptual difficulty, the physical meaning of  $\partial P_p / \partial x_i$  is less clear because of the discrete nature of the solid phase. Modelling such a pressure is problematic, owing to the uncertainty in its definition and the difficulties involved in its measurement.

The particle pressure can be defined from the trace of the particle-phase stress

tensor. Hence, the physical mechanisms incorporated into the particle pressure can be gleaned from components of the stress tensor. For rapid granular flows (Campbell 1990), in which the effect of the interstitial fluid is negligible, two contributions to the stress can be identified: the ‘streaming’ or Reynolds stress and the collisional contribution to the stress. The streaming component of the stress appears as a result of the momentum transfer due to the fluctuating velocity of the particle phase. The collisional stress reflects the momentum transfer between particles during a collision. In concentrated mixtures, stresses can also be generated due to enduring contacts between particles. Force chains appear and stresses are transmitted through the bulk of the mixture over distances of many particles (Lui *et al.* 1995). When the interstitial fluid is not negligible, a hydrodynamic contribution to the particle stress tensor is added to account for the drag or added mass of the particles (Nott & Brady 1994; Bulthuis, Prosperetti & Sangani 1995; Tsao & Koch 1995; Sangani *et al.*, 1996). Contributions to the stress due to non-hydrodynamic interactions can occur when there are other inter-particle forces such as colloidal forces or those due to electrostatic charging.

Over the past thirty years there have been several attempts to model the constitutive behaviour of two-phase mixtures including the particulate-phase pressure. Early attempts simply assumed the particle pressure to be equal to the fluid pressure (Wallis 1969), or equated it to zero due to its supposed negligible effect (Jackson 1963).

More recently, the significance of this quantity has been encountered in the context of stability of fluidized beds. Studies have shown that the gradient of the particle pressure is a dominant factor in determining the stability of the mixture (Jackson 1985; Batchelor 1988; Foscolo & Giliardo 1987; Jin 1996) because of its dependence on the local concentration gradients within the flow. Some researchers recognized that it could be generated by particle collisions (Needham & Merkin 1983), but owing to a lack of experimental evidence they assumed it to be a simple function of the void fraction,

$$P_p = P_o v \quad (1.1)$$

where  $P_o$  is a constant and  $v$  is the solid volume fraction of the mixture.

In the work by Batchelor (1988), the governing equations for the mean motion of particles in a fluidized bed are formulated based on one-dimensional control volume analysis. All of the parameters within the model are linked on physical arguments to the two dependent variables – the local solids concentration,  $v$ , and the superficial fluid velocity,  $u_o$  (referred to by Batchelor as the local mean particle velocity according to the frame of reference used in his paper). The volume-averaged model introduces a closure problem; hence, the term in the governing equation that involves the square of the velocity fluctuations,  $\langle v^2 \rangle$ , must be related to the local mean velocity and the solids concentration. Batchelor assumes that in a homogeneous bed,  $\langle v^2 \rangle = F(v)u_o^2$ , where  $F(v)$  is some function of solids fraction. The function  $F(v)$  is assumed to approach 0 for two limiting cases: as  $v$  approaches 0, and as  $v$  approaches the close-packed limit. The first limit is due to the absence of velocity fluctuations as the number of particles approaches zero; the second limit for high solids concentration results from the decrease of fluctuations as particles approach a dense state. Batchelor also argued that the representation for  $\langle v^2 \rangle$  would depend on the local gradients of solids concentration and mean velocity for non-homogeneous flows. In the governing equations the term  $mn\langle v^2 \rangle$ , where  $m$  and  $n$  are the particle mass and number density, corresponds to the mean normal stress in an ideal gas of molecules. Hence, Batchelor’s

representation for the collisional particle pressure in a homogeneous bed is

$$P_p = v \rho_p F(v) u_o^2 \tag{1.2}$$

where  $\rho_p$  is the density of the particles. Using the simplest representation for  $F(v)$  to satisfy the limiting conditions on  $v$ , Batchelor suggested the following representation:

$$F(v) \approx \frac{v}{v_{cp}} \left( 1 - \frac{v}{v_{cp}} \right)$$

where  $v_{cp}$  is the closed-packed solid fraction ( $v_{cp} \approx 0.62$  for a randomly packed bed of uniform sized particles).

Besides the work of Batchelor, the stability work by Foscolo & Gibilaro (1987) can also be used to find a representation for the particle pressure. They introduce a force that is applied to the particles due to the particulate nature of the fluidized bed. This force depends on the ‘particle-phase pressure’ and is calculated from fluid dynamic considerations. The value of the particle-phase pressure can be determined by integrating the particle-phase pressure gradient given by Foscolo & Gibilaro. Using their terminology the pressure is written as

$$P_p = v^2 \rho_p u_e^2 \tag{1.3}$$

where  $u_e$  is the ‘elastic wave velocity’ and is defined as

$$u_e = \left( 3.2 g d_p \frac{\rho_p - \rho_f}{\rho_p} \right)^{1/2} \tag{1.4}$$

where  $\rho_f$  is the density of the fluid phase,  $g$  is the acceleration due to gravity and  $d_p$  is the diameter of a particle.

Based on modifications to kinetic theory to include the effects of the interstitial fluid, Koch (1990) and Buyevich & Kapbasov (1994) analysed fluidized systems. In the study by Koch, expressions for the particle-phase stress, as a function of the particle Stokes number, are obtained for the case of dilute mixtures. The particle pressure is expressed as

$$P_p = \rho_p v T \tag{1.5}$$

where  $T$  is particle fluctuating ‘temperature’,

$$T = G(v) St^{-2/3} (u_p - u_f)^2$$

and  $St$  is the particle Stokes number defined as  $St = m(u_p - u_f)/(6\pi\mu(\frac{1}{2}d_p)^2)$ ,  $u_p$  and  $u_f$  are the ensemble-averaged particle and fluid velocities respectively, and  $G(v)$  is a function of the solid fraction.

The fluidized bed work by Buyevich & Kapbasov (1994) introduces a volume-averaged model. Similar to the work by Koch, the particle pressure is linked to the square of the velocity fluctuations, or the granular ‘temperature’. Hence, similarly to kinetic theory, the particle pressure is equated to the fluctuation temperature,  $T$ ,

$$P_p = \rho_p T H(v) \tag{1.6}$$

where the function  $H(v)$  is the particle distribution function used in dense-gas kinetic theory analyses, such as the Carnahan–Starling or the Enskog representations. The authors solve explicitly for the normalized fluctuation temperature as a function of the solids concentration in a macroscopically uniform mixture. The particle pressure

from this study can be written in a form similar to that developed by Batchelor,

$$P_p = \nu \rho_p H'(v) u_o^2, \quad (1.7)$$

where the function  $H'(v)$  is determined from the choice of the particle distribution function and the calculations for the particle temperature.

In addition to the analyses for fluidized beds, the particle pressure term has also been encountered in studies involving turbulent solid–fluid mixtures (Abu-Zaid & Ahmadi 1995; Ahmadi & Ma 1990; Ahmadi 1985). In the dispersed mixture work by Abu-Zaid & Ahmadi (1995), the authors use the following relation for the mean particle pressure:

$$P_p = \frac{P_f v}{1 - v} \quad (1.8)$$

where  $P_f$  is the mean interstitial fluid pressure. This expression is applicable when the particles are not in direct contact except during short collisional periods.

Despite the theoretical studies described above there have been few attempts to measure the particle pressure experimentally, primarily because of a lack of experimental techniques that provide a reliable measurement of this quantity. In a study of gas fluidized beds Campbell & Wang (1990) used a capacitance probe, which measured the difference between the total pressure and the gas pressure, and hence measured the average pressure generated by the particles. They concluded that the granular pressure results from agitation generated by the rising bubbles that appear in gas-fluidized systems. The bubbles cause the movement of many particles towards the container walls, thus generating a pressure. This description would not hold for a liquid-fluidized system since bubbles generally do not appear.

The first attempt to measure the particle pressure in a liquid-fluidized bed was by Kumar, Hart & Brennen (1990). They used a flush-mounted hydrophone to record the collisions of particles with the face of the hydrophone. The calibration of their hydrophone was not satisfactory. However, some of the qualitative phenomena were clearly captured in their results.

The measurement of the granular pressure is also of practical importance. The random motion of particles can have a strong effect on the erosive potential of the flow, for example in slurry pumps and pipes (Roco & Addie 1987). Also the interactions between particles and with containing walls could cause particle breakage or surface roughness modification, and therefore cause a change of physical (and possibly chemical) attributes of the particles. The particle pressure may also affect the heat transfer characteristics of the flow. For example fluidized beds are often used as heat exchangers because of the intense mixing that occurs naturally in these systems. The rate of heat transfer is governed by the frequency of particle contacts with the walls (Ben-Ammat, Kaviany & Barber 1992).

The present paper describes a new technique for measuring the collisional particle pressure in particulate solid–liquid systems using a high-frequency-response dynamic pressure transducer that measures the collisions of individual particles with the walls. Since only the pressure fluctuations from particle collisions are measured, the particle pressure represents the collisional particle pressure. Time-averaged granular pressures are measured for various flow conditions and concentrations and for different particle sizes and densities. An estimate of the particle impact velocity is calculated from the measurement of the collisional impulse. The results are also used to quantify the contribution to the granular pressure due to direct contacts and the contribution due to collisions within the medium that is transmitted through the fluid.

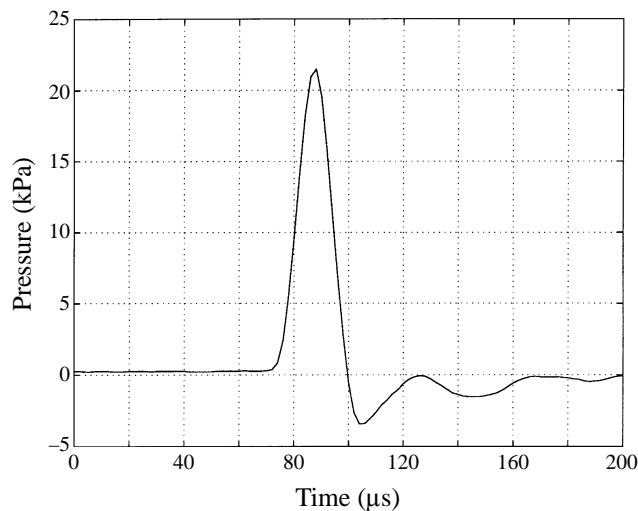


FIGURE 1. Typical pressure pulse generated by a particle collision.

## 2. Experimental setup

Typically collisions of particles with the wall have a duration of tens of microseconds; therefore, to record such events, it is necessary to use a device with a very high frequency response. The current experiments use a piezoelectric dynamic pressure transducer manufactured by PCB Piezotronics, which can respond to changes in pressure lasting up to two microseconds. It has an active surface of 3.75 mm diameter. A typical signal resulting from a collision is shown in figure 1. It consists of a positive spike (of 22  $\mu\text{s}$  of duration in this case), followed by a decaying oscillation, which is probably the result of the dynamics of the membrane. For the experimental measurements two different pressure transducers with similar characteristics were used.

Experiments were performed in the facility shown in figure 2. Two different circular test sections with internal diameters of 10.16 cm and 5.08 cm were used. The working section was fabricated out of transparent lucite to facilitate the visual observation of the flowing mixtures. Prior to an experiment the particles were stored in a bin on top of the working section. By setting the aperture of the controlling solids cylinder and the downstream water valves, different flow conditions could be generated. Both cocurrent and countercurrent flows were obtained for a wide range of solid fractions. Also, by installing a screen and a flow straightener at the bottom of the working section, the system was also operated as a fluidized bed. The particles employed were all nearly monodisperse spherical particles. Properties of the particles are listed in table 1. The solid fraction was monitored using an impedance volume fraction meter (IVFM) developed by Bernier (1982) and Kytömaa & Brennen (1986). This device measured the instantaneous impedance of the flowing mixture, which is proportional to the volume fraction of the non-conducting disperse phase averaged over the cross-section; the calibration of this device was obtained as described by Kytömaa & Brennen (1986). The instrumentation is shown in figure 3.

The data acquisition system was started once the system had reached a steady state. The signal obtained from the transducer was high-pass filtered and amplified and then input to a trigger box and to a computerscope data acquisition system mounted in a PC. Pressure fluctuations below 1 KHz were filtered out completely, thus only

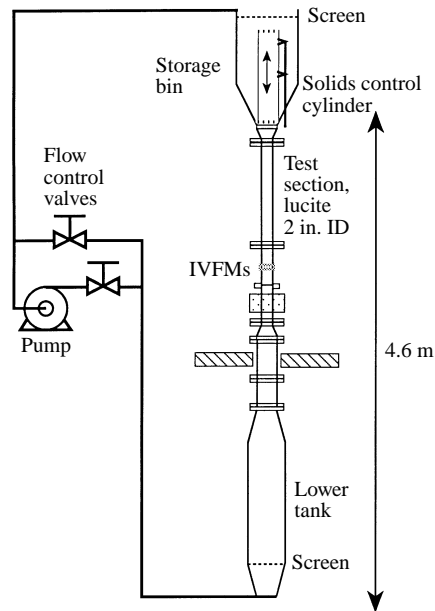


FIGURE 2. Experimental setup.

Material	$d_p$ (mm)	$\rho_p/\rho_f$	$u_t$ (cm s <sup>-1</sup> )	$Re_t$	$n$
Glass +	2.06	2.54	22.7	452	2.39
Glass ×	3.00	2.54	31.8	954	2.40
Glass *	3.96	2.54	36.8	1338	2.40
Glass ○	6.00	2.54	47.4	2583	2.40
Steel ⊕	4.50	7.78	89.6	3665	2.40
Nylon ⊗	6.35	1.14	13.6	785	2.40
PVC ⊙	3.41 †	1.43	16.0	440	2.44

† Equivalent diameter, cylindrical shape.

TABLE 1. Properties of particles used in experiments

the pressure pulses generated by the collisions of particles were detected with the present setup. To eliminate the collection of background noise a threshold level had to be chosen, and this was set in the trigger box. When the signal from the transducer was higher than the threshold level the trigger box activated the data acquisition card and the signal was stored in the computer's memory. A software program then calculated, in real time, the maximum pressure, impulse and duration of the collision, stored the results and reset the data acquisition card, allowing the data acquisition system to take measurements in a continuous manner. The event rate was measured independently with a counter that indicated the number of times the signal exceeded the threshold level in a given time period.

As expected for large dense particles, the experiments exhibited important concentration fluctuations in the form of voidage waves (Harrison, Davidson & deKock 1961). As the concentration of the bed decreased, the solid fraction fluctuations became more random, and the voidage waves were difficult to discern. These waves do

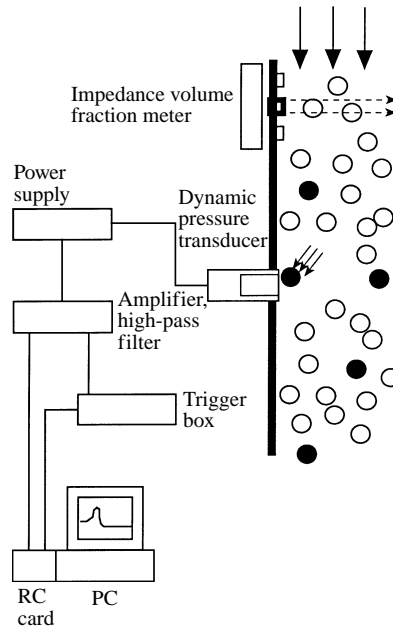


FIGURE 3. Experimental setup: instrumentation.

not contribute directly to the granular pressure, though the shearing they imply may add to the production of random granular motions.

The time-average particle pressure is calculated as

$$P_p = \dot{s} I_m \quad (2.1)$$

where  $\dot{s}$  is the event rate and  $I_m$  is the average impulse. The impulse is

$$I = \int_0^\tau P(t) dt \quad (2.2)$$

where  $P(t)$  is the pressure signal produced during an individual impact, and  $\tau$  is the duration of the collision. An estimate of the impact velocity,  $u_i$ , can be calculated from

$$u_i = F_m \tau / m \quad (2.3)$$

where  $F_m$  is the maximum force exerted on the transducer during an individual collision and  $m$  is the mass of the particle. The maximum force is calculated by multiplying the measured maximum pressure  $P_m$  by the area of the sensitive surface of the transducer,  $A_{tr}$ . Sets consisting of at least 100 collisions (normally more) were used to calculate the average values of granular pressure and impact velocity, which were made over a time period in the order of hundreds of seconds. By taking consecutive measurements under the same nominal experimental conditions, the repeatability was verified.

The pressure transducers were installed at different axial locations in the working section to determine the axial variations in the particle pressure. No significant change with axial location was detected for the flowing mixture. In the case of the fluidized bed some variation occurred when the transducer was less than one test section diameter above the bottom of the bed.

The accuracy and calibration of the pressure transducer were verified by comparing

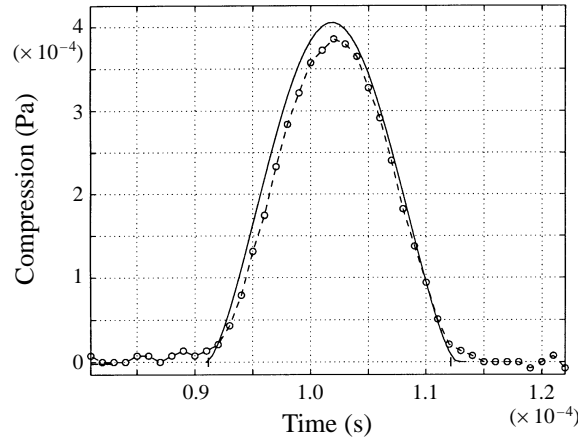


FIGURE 4. Calibration of the pressure transducer. Direct comparison of experimental collision in air (o) with Hertzian prediction (—).  $u_i = 75 \text{ mm s}^{-1}$ .

the output collision signals with predictions from the Hertzian theory of contact. Hertzian theory (see for example Goldsmith 1960) predicts the duration and the maximum compression force during a collision as a function of impact velocity and particle properties. For a sphere impacting a flat surface, the maximum compression force is

$$F_m = 0.706 \left( \frac{u_i^6 m^3 d_p}{(k_1 + k_2)^2} \right)^{1/5} \quad (2.4)$$

where  $k_j$  is

$$k_j = \frac{1 + \alpha_j^2}{\pi E_j} \quad (2.5)$$

and  $u_i$  is the impact velocity,  $E_j$  is the Young's modulus of elasticity for material  $j$  and  $\alpha_j$  is the corresponding Poisson's ratio. The collision duration is

$$\tau = 7.894 \left( \frac{m^2 (k_1 + k_2)^2}{d_p u_i} \right)^{1/5}. \quad (2.6)$$

Therefore, the collision impulse (as defined by (2.2)) is

$$I = 2.047 \frac{u_i m}{A_{tr}}. \quad (2.7)$$

Hence, from Hertzian theory, the magnitude of the collision impulse does not depend on the elastic properties of the surfaces in contact.

A simple calibration device was constructed involving a pendulum consisting of a glass particle and a fine string. The particle was positioned initially such that a controlled direction and velocity of impact could be applied to the transducer. The measured collision characteristics in air were compared with the Hertzian predicted values by calculating the impact velocity from the pendulum equation (neglecting the effect of air) and using tabulated material properties (Avalone & Baumeister 1986). Figure 4 shows a comparison of the compression pressure as a function of impact time for a 3 mm glass particle. The Hertzian predictions use a value of  $\alpha = 0.22$  and  $E = 50.5 \text{ GPa}$  for the glass particles. Figures 5 and 6 present the calibration measurements of the impact pressure and duration of collision and the comparison



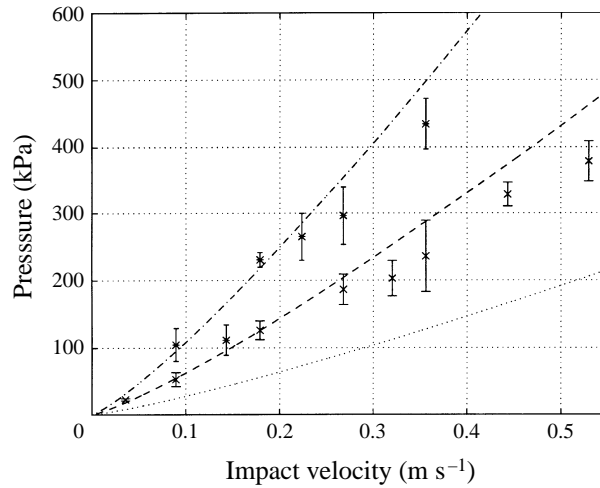


FIGURE 5. Calibration of the pressure transducer. Impact pressure as a function of impact velocity and particle diameter. Experimental (in air):  $\times$ , 3 mm glass bead;  $*$ , 4.2 mm glass bead. Hertzian predictions:  $\cdots$ , 2 mm glass bead;  $---$ , 3 mm glass bead;  $- \cdot -$ , 4.2 mm glass bead.

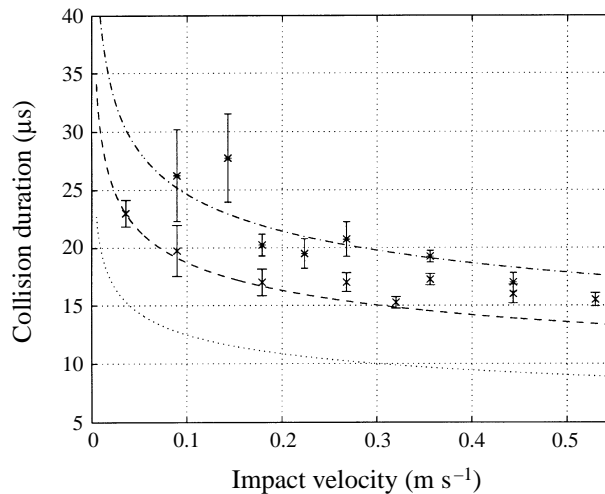


FIGURE 6. Calibration of the pressure transducer. Duration of collision as a function of impact velocity and particle diameter. Experimental (in air):  $\times$ , 3 mm glass bead;  $*$ , 4.2 mm glass bead. Hertzian predictions:  $\cdots$ , 2 mm glass bead;  $---$ , 3 mm glass bead;  $- \cdot -$ , 4.2 mm glass bead.

with the predictions from Hertzian theory. A perfect match is not expected due to the many assumptions in the development of Hertzian theory. The Hertzian model was used to confirm the nature and magnitude of the forces occurring during a collision. Based on these comparisons the manufacturer's calibration was used in the subsequent analysis of the data.

### 3. Liquid-fluidized bed experiments

The granular pressures measured in the fluidized bed are shown in figure 7 as a function of the solid fraction for glass particles with four different diameters. These tests were all performed in the small diameter test section (5.1 cm). For a dilute

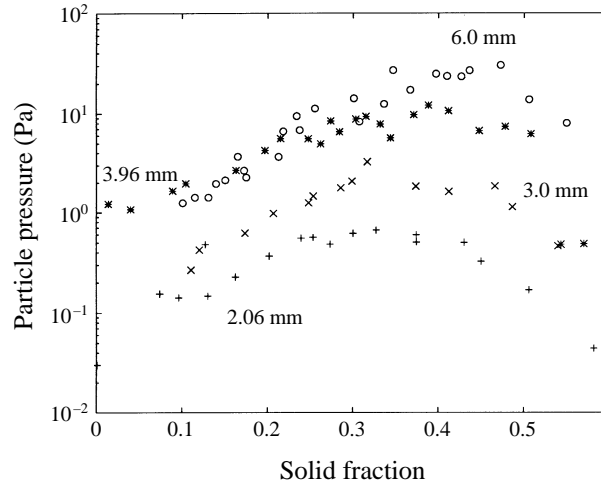


FIGURE 7. Particle pressure  $P_p$  as a function of the solid fraction  $v$  for fluidized glass particles in the 5.1 cm test section.

system, at low concentrations, the value of the particle pressure is low. In this regime the particles are free to move and collide sporadically; therefore few particles collide with the transducer per unit of time, making the event rate small. On the other hand, at high solid fractions collisions are more likely to occur. However, owing to the high concentration, these collisions occur at very small velocities producing low-impulse collisions, which result in a low value of the particle pressure. At intermediate concentrations (from 30% to 35%) the particle pressure reaches a maximum. In this range the impact velocity is higher than in the concentrated case, and the event rate is higher than in the dilute case. The combination of these two competing mechanisms results in a maximum particle pressure for these intermediate concentrations.

The value of the particle pressure is a function of the particle size, being higher for larger particle diameters. The maximum pressure is located at slightly higher concentrations for larger particles. Figure 8 shows the particle pressure as a function of the superficial velocity of the fluid  $u_o$ . The velocity  $u_o$  is calculated using the Richardson–Zaki relation

$$u_o = u_t(1 - v)^n \quad (3.1)$$

where  $n$  is an empirically determined parameter which depends on the terminal Reynolds number of the particle,  $Re$ . Table 1 includes the values of  $n$  for the particles used in these experiments. The validity of equation (3.1) was verified the present experimental setup, with agreement between measured and calculated velocities within  $\pm 6\%$ . Since the volume fraction can be measured more accurately, the calculated value of  $u_o$  is used instead for convenience. As shown in figure 8, above the minimum fluidization velocity the measured value of the particle pressure increases rapidly. After reaching a maximum value for some intermediate velocity, the granular pressure decreases again and tends to zero as the superficial velocity approaches the value of the terminal velocity.

A plot of the average impact velocity (normalized by the terminal velocity,  $u_t$ ) as a function of the solid fraction is shown in figure 9 for glass particles in the 5.2 cm diameter test section. Even with substantial scatter, the smaller particles tend

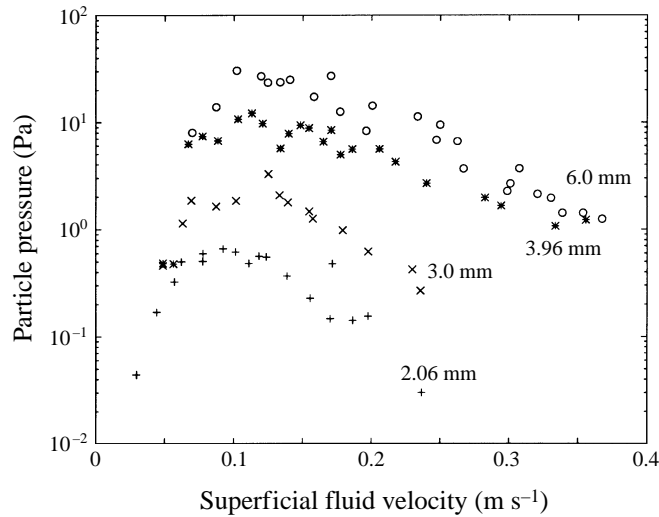


FIGURE 8. Particle pressure  $P_p$  as a function of the superficial fluid velocity  $u_o$  for fluidized glass particles in the 5.1 cm test section.

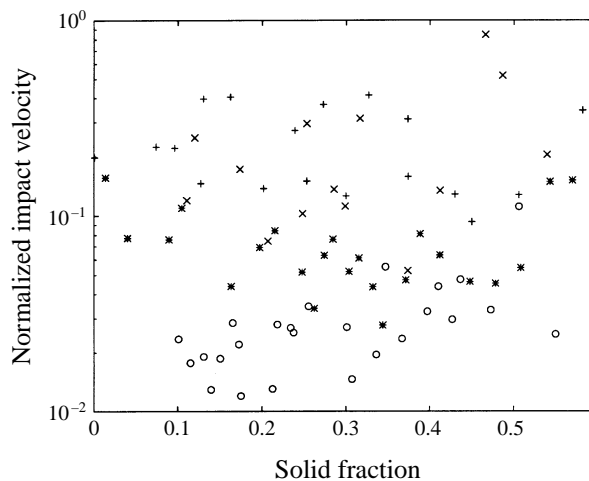


FIGURE 9. Calculated impact velocity  $u_i$  as a function of the solid fraction  $v$  for fluidized glass particles in the 5.1 cm test section. For symbol identification see table 1.

to collide at higher velocities than larger particles. The impact velocity does not appear to have a consistent trend when plotted as a function of the solid fraction. All collision velocities are below the terminal velocity.

Some of the features of fluidized systems are believed to be determined by the geometry and dimensions of the container (Kytömaa & Brennen 1986). To investigate the dependency of the granular pressure on the dimensions of the bed, tests were conducted in the two different test sections. A comparison of the granular pressures is presented in figure 10 as a function of the solid fraction. To enable the comparison the two plots are presented side by side, and only the results for glass spheres are shown. The difference between the two cases is not significant, although the amount

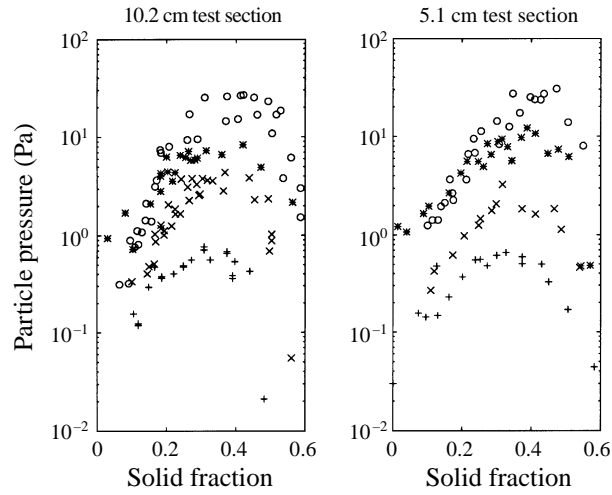


FIGURE 10. Particle pressure  $P_p$  as a function of the solid fraction  $v$ . A comparison of the pressures measured in a 10.2 cm and a 5.1 cm test section. Fluidized glass particles. For symbol identification see table 1.

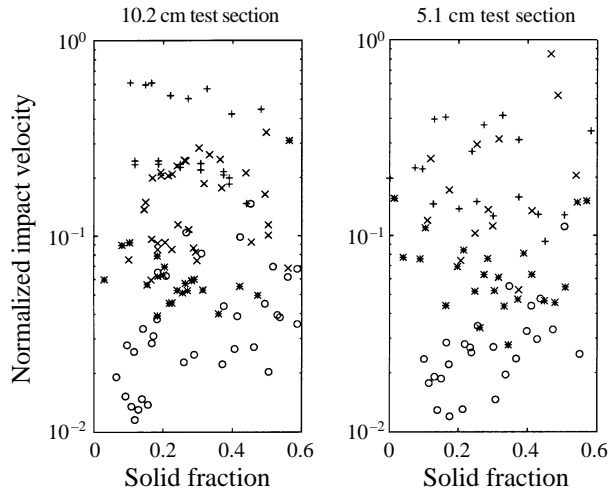


FIGURE 11. Calculated impact velocity  $u_i$  as a function of the solid fraction  $v$ . A comparison of the calculated impact velocities in a 10.2 cm and a 5.1 cm test section. Fluidized glass particles. For symbol identification see table 1.

of scatter is slightly higher for the larger test section. Figure 11 shows a comparison of the calculated impact velocity for the two test sections. The trends seem similar.

Experiments were also performed using particles of different densities. Figure 12 shows the particle pressure measured for steel particles of 4.5 mm diameter in a 5.1 cm test section. For comparison, the results are presented along with the measurements obtained for 3 mm and 4 mm diameter glass particles. Again, the more massive particles produce higher particle pressures. In figure 13 measurements for nylon spheres of 6.35 mm diameter and 3.43 mm PVC rods are shown along with the results for 6 mm, 3 mm and 4 mm glass spheres. Clearly, the granular pressure is higher for particles with greater density.

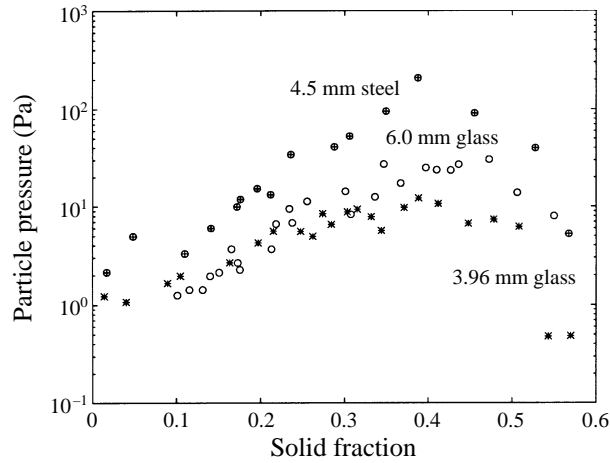


FIGURE 12. Particle pressure  $P_p$  as a function of the solid fraction  $v$ . A comparison of particles with different densities for fluidized steel and glass particles in the 5.1 cm test section.

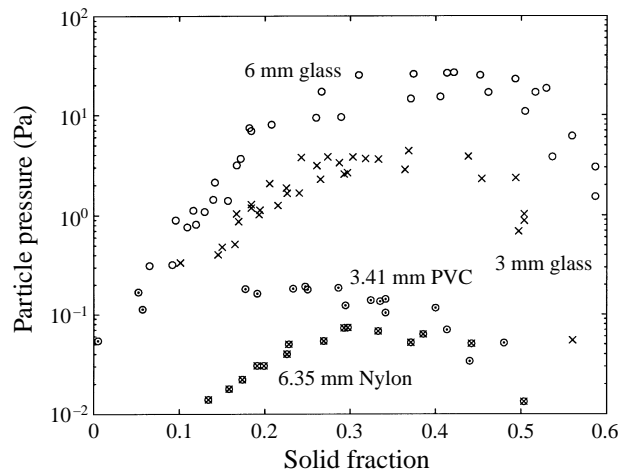


FIGURE 13. Particle pressure  $P_p$  as a function of the solid fraction  $v$ . A comparison of particles with different densities for fluidized plastic and glass particles in the 10.2 cm test section.

#### 4. Probability density functions

A detailed statistical analysis of the measured collisions was also conducted. Sets of 1000 events (or more) were taken at a number of solid fractions to provide enough information to construct graphs of the probability density functions (PDF), or histograms of the occurrence of the individual collisional pressures, durations and impulses. Figures 14, 15 and 16 show the normalized probability density functions obtained for 3 mm glass particles in a 10.2 cm test section. The probability density functions are normalized such that

$$\int_0^{\infty} p\{x\}dx = 1.$$

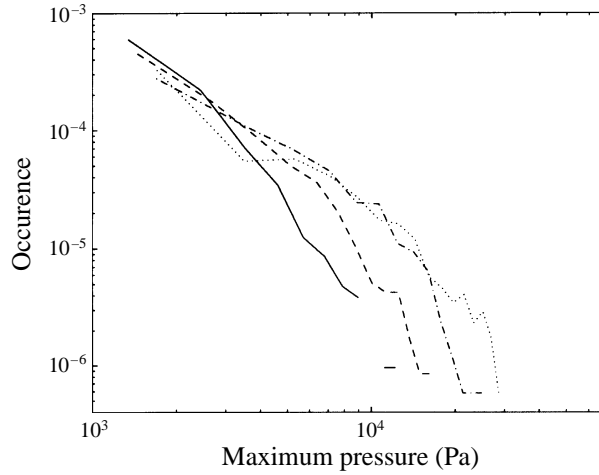


FIGURE 14. Probability density function of individual collision pressure. Fluidized glass 3 mm particles in a 10.2 cm test section. —,  $v = 0.503$ ; ---,  $v = 0.438$ ; - · -,  $v = 0.318$ ; · · ·,  $v = 0.194$ .

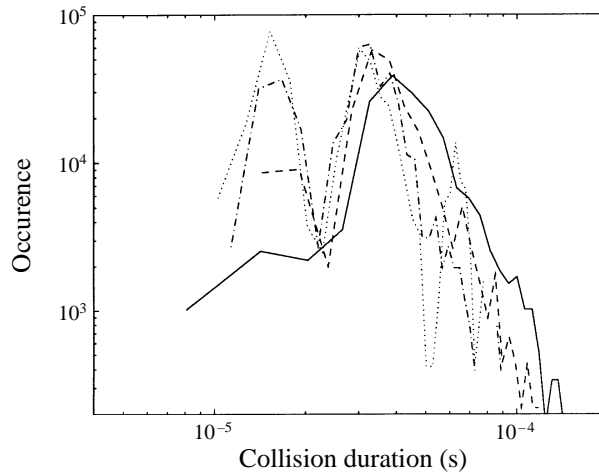


FIGURE 15. As figure 14 but for collision duration.

Although these figures show the results of just one experiment, the repeatability was verified by taking consecutive sets of data points; once processed, the results obtained were practically identical.

Figure 14 presents the PDF of the collisional pressure. Clearly, low-pressure collisions occur more frequently than high-pressure collisions for all solid fractions. The value of the lowest pressure in the plot is the threshold level chosen for that experiment. The distribution becomes wider for lower solid fractions. In other words, more high-pressure impacts occur in a dilute bed.

Figure 15 shows the PDF of the collision duration. For all the solid fractions tested the PDF shows a distribution with two distinct peaks. The first peak (short-duration collisions) occurs at approximately 15  $\mu\text{s}$  and its magnitude appears to be a function of the solid fraction. The second peak (long-duration collisions) occurs at approximately 37  $\mu\text{s}$ , and becomes narrower for lower solid fractions. During the calibration of

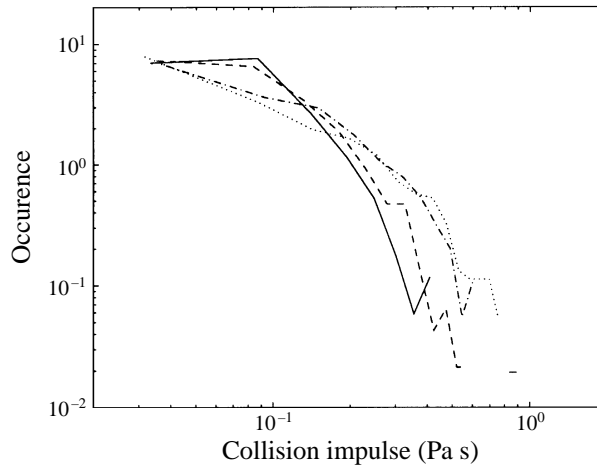


FIGURE 16. As figure 14 but for collision impulse.

the pressure transducer (which utilized normal impacts) *only* collisions of the long-duration type were encountered. The duration of these collisions is in accord with the Hertzian predictions. The short-duration collisions cannot be Hertzian: if the impact velocities were higher during the short-duration collisions, the maximum pressure would also increase. However, the experimental results indicate that the short-duration collisions are associated with low-pressure collisions for the glass spheres.

Figure 16 shows how the distribution of collision impulse changes with solid fraction. In a concentrated bed, collisions of low impulse are predominant. As the solid fraction decreases the average impulse of the collision increases. The distribution becomes wider, indicating an increase in the occurrence of higher impulse collisions.

The same phenomena and trends are found for different particle diameters and densities. The magnitudes of individual collision pressures and collision impulses appear to be scaled with the particle mass. The two distinct peaks in the PDF of the collision duration occurred for all of the particles tested. The peaks occurred at different locations depending on the mass of the particles tested. The collision duration for the two types of pressure pulses (for the glass particles) varies with particle diameter according to

$$\left. \begin{aligned} \frac{\tau_{2mm}^{sh}}{\tau_{3mm}^{sh}} &\approx \frac{\tau_{2mm}^{lg}}{\tau_{3mm}^{lg}} \approx \frac{d_{2mm}}{d_{3mm}} \approx 0.666, \\ \frac{\tau_{2mm}^{sh}}{\tau_{4mm}^{sh}} &\approx \frac{\tau_{2mm}^{lg}}{\tau_{4mm}^{lg}} \approx \frac{d_{2mm}}{d_{4mm}} \approx 0.5, \end{aligned} \right\} \quad (4.1)$$

where the subscripts denote the particle diameter and the superscripts denote the type of collision (short or long). For a more detailed analysis see Zenit (1997).

Figure 17 shows a comparison between the total particle pressure (solid line) and the contribution to the particle pressure from the long-duration collisions (dashed line). This plot shows typical results obtained for 3 mm glass particles in the 10.2 cm test section. It is important to note that though the short-duration collisions may have occurred as frequently as the long-duration collisions, their contribution to the average particle pressure was less than 5% for glass particles for all solid fractions.

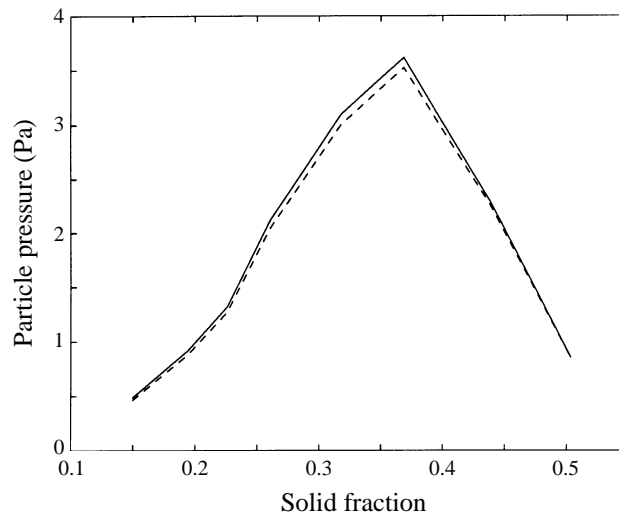


FIGURE 17. Particle pressure as a function of solid fraction: a comparison between the total particle pressure (—) and the particle pressure generated solely by the long-duration collisions (- -). Fluidized glass 3 mm particles in a 10.2 cm test section.

### 5. Vertical gravity-driven flow

In a fluidized bed the net velocity of the particulate phase is zero and this lack of mean motion may affect the granular pressure. To investigate this possibility, measurements of the particulate pressure were also performed for a vertical flow in a mixture of glass particles in water. In all cases the net velocity of the solid phase is downwards. The motion of the liquid could be either downwards (cocurrent with the particles) or upwards (in a countercurrent configuration).

Figure 18 presents the granular pressure measured for a flowing mixture under two flow conditions, cocurrent and countercurrent flows, and in both test sections. Figure 19 shows the calculated impact velocities. Both the impact velocities and the particle pressures obtained for these cases have a wider spread than in the case of fluidized beds. Therefore the variation of the particle pressure with respect to solid fraction is not as clear as in the case of a fluidized bed. In fact, the particle pressure remains fairly constant over the entire range of solid fraction, reaching a maximum around  $\nu = 0.30$ . Hence the net motion of the solid phase in the mixture causes different trends in the particle pressure. The magnitude of the pressures in the gravity-driven flows is approximately equal to the maximum value found in the fluidized bed for the same particle size. Moreover, the direction of motion of the fluid phase does not appear to have a significant influence on the magnitude of the measured particle pressure.

### 6. Discussion

The measurements of the particle pressure obtained in this study correspond to the contribution from particle collisions. Since the experimental setup registers high-frequency events, the experimental measurements only include the collision-based contributions to the particle pressure.

Figures 12 and 13 show the large differences in the magnitude of the particle pressure for particles of different density and size. For example, at a solid fraction



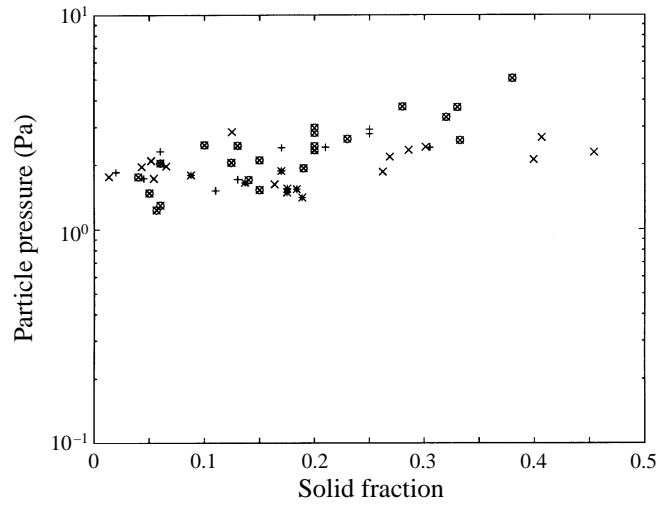


FIGURE 18. Particle pressure  $P_p$  as a function of the solid fraction  $v$ . Vertical gravity-driven flow of 3 mm glass particles.  $\times$ , cocurrent flow in 5.1 cm test section (TS);  $*$ , countercurrent flow in 5.1 cm TS.  $\otimes$ , cocurrent flow in 10.2 cm TS;  $+$ , countercurrent flow in 10.2 cm TS.

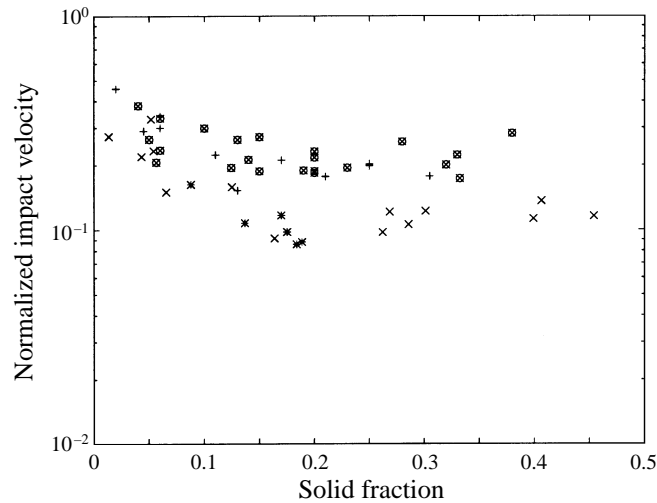


FIGURE 19. Calculated impact velocity  $u_i$  as a function of the solid fraction  $v$ . Vertical gravity-driven flow of 3 mm glass particles. Symbols as for figure 18.

of 0.4, the particle pressure for the 4.5 mm steel spheres is more than 3 orders of magnitude larger than the particle pressure for the 6.35 mm nylon spheres. Clearly the particle pressure must increase with the ratio of the density of the particles,  $\rho_p$ , to that of the surrounding fluid,  $\rho_f$ . In addition, the pressure must also depend on the velocity of the particles. Hence, an appropriate scaling of the particle pressure would be a particle dynamic pressure based on the particle density,  $\rho_p$ , and a characteristic velocity,  $u_t$ . Figure 20 presents a plot of the particle pressure normalized by  $\frac{1}{2}\rho_p u_t^2$  for all of the types of particles as a function of the solid fraction. As observed from the figure, the difference between the normalized particle

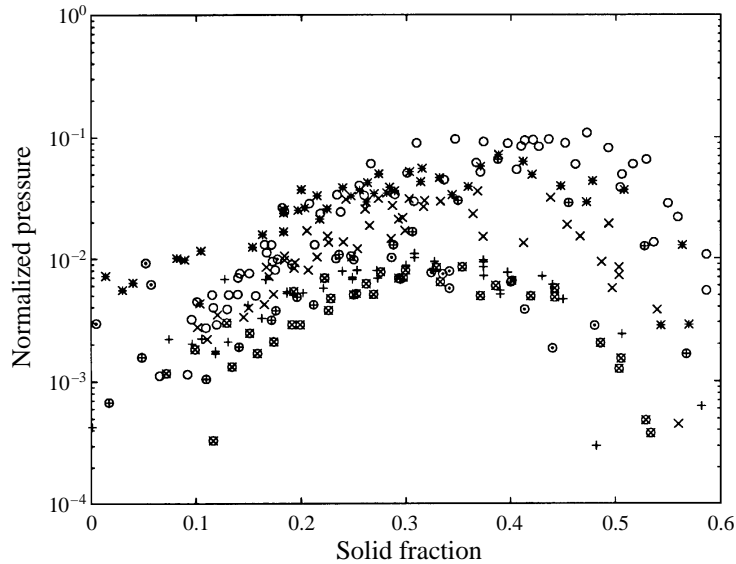


FIGURE 20. Non-dimensional particle pressure  $\hat{P}_p$  as a function of solid fraction  $v$ . Pressures normalized by  $\frac{1}{2}\rho_p u_t^2$ . Results for all particles and tests sections in a fluidized bed.

pressure for the 4.5 mm steel spheres and the 6.35 mm nylon spheres is less than an order of magnitude at a solid fraction of 0.4. Hence, the choice of the particle dynamic pressure appears to be the correct scaling for the particle pressure. However, there are still considerable differences in the normalized pressure for the different types of particles. One observation is that the higher the terminal Reynolds number, the greater the normalized pressure at a given solid fraction. The exception to this observation, however, is the steel spheres. This result may indicate that in addition to the solid fraction and the terminal Reynolds number, the normalized pressure may also depend on the ratio of the density of the solid phase to that of the fluid, or the local Reynolds number. This dependency is certainly suggested in the work by Batchelor (1988). In addition the pressure might be affected by the voidage waves that are present at high concentrations and higher density particles.

While the measurements obtained with the vertical flow have approximately the same magnitudes as in the fluidized bed there are some notable differences. In addition, there were also some experimental limitations that may have influenced the results. It was not possible to generate highly concentrated flowing mixtures (>45%) in the present facility, and only low concentrations were possible for the case of countercurrent flows (< 25%). Furthermore, the number of individual collisions collected per test was limited by the running time of the experiment since only a finite mass of particles could be stored in the bin. Therefore for some conditions the experiment could only be operated for a few minutes. These factors contributed to the larger scatter encountered in particle pressures for the case of flowing mixtures.

In the gravity-flow experiments, the short-duration pressure pulses were, in general, more frequent than in the fluidized bed experiments. The short-duration events constituted up to 75% of the total number of events in the gravity-flow experiments compared to a maximum of 50% in the fluidized beds. In addition the particle pressure was not affected by the direction of the fluid flow.

In the analysis of the probability density functions of collision duration two different

characteristic pressure pulses are encountered: a long-duration pulse whose duration and strength corresponded to those predicted by the Hertzian theory of contact, and a short-duration pulse whose duration and strength are not in accord with Hertzian predictions. Several features of the short-duration pulses are evident from the particle pressure measurements: their strength and duration are both smaller than those predicted by Hertzian theory; their occurrence increases as the solid fraction decreases (for the case of a fluidized bed); they occur at least as often as the long-duration collisions (for the case of vertical flows); they are not observed when calibrating the transducers.

The origin of the short-duration pulses was not resolved until a detailed visualization of the particles was performed. An observation window was installed near the pressure transducer. A high-speed digital camera, able to record images as fast as 500 frames per second, was positioned to observe the face of the transducer. The camera was synchronized with the data acquisition system so that images of the events occurring on the face of the transducer were filmed at the moment at which a pressure pulse was sensed. With this setup the pressure pulse obtained could be correlated with the motion of the particles interacting with the transducer. Clear images of the motion of the particles interacting with the transducer could, however, only be obtained for dilute fluidized beds. Many long and short pressure pulses were recorded and analysed.

The long-duration pulses were confirmed to be the result of direct contacts with particles against the transducer. Particles were observed to collide with the face of the transducer at many different speeds and incident angles. The strength and duration of these collisions were confirmed to be in accordance with Hertzian predictions.

The short-duration events were found to be produced not by actual contacts between particles and the transducer, but rather by collisions between particles in the bulk that occur in the vicinity of the pressure transducer without having physical contact with it. The pressure pulse produced by the collision travelled from the point of occurrence to the transducer through the interstitial fluid. The intensity of these pulses appeared to be related to the impact velocity of the collision, the orientation of the colliding particles with respect to the transducer and the distance from the collision to the transducer. The duration of these events was determined by the fact that two particles are colliding rather than a single particle with a flat surface. A detailed analysis of the nature of these pressure pulses can be found in Zenit (1997).

If the collisional particle pressure is an additional pressure generated by collisions of the particles, it can be concluded from these observations that the pressure is generated by direct impacts of particles, and by pressure pulses transmitted through the fluid due to particle–particle interactions.

## 7. Comparison with existing models

As mentioned in the Introduction, several models have been proposed for the particle pressure. Figures 21 and 22 present a direct comparison with some of these models. To facilitate the comparison only the results obtained for 3 mm particles in a fluidized bed are presented. The pressure data are presented in non-dimensional form, where the pressure is normalized by

$$\hat{P}_p = \frac{P_p}{\frac{1}{2}\rho_p u_t^2}.$$

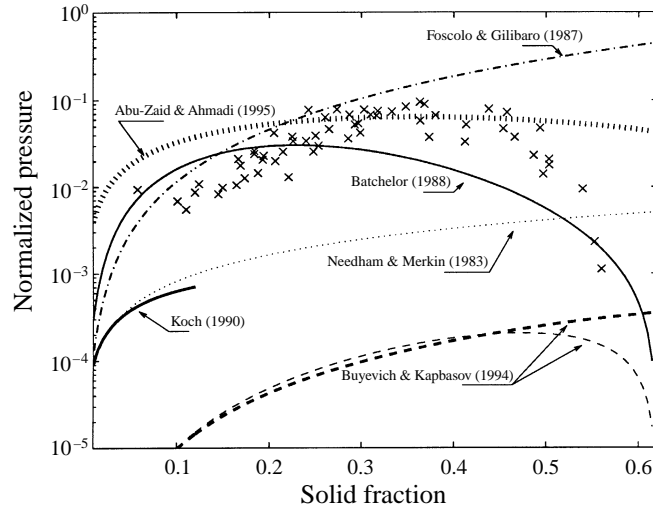


FIGURE 21. Comparison of the experimental results with theoretical models. Experimental results for 3 mm glass particles in a fluidized bed ( $\times$ ). Pressures normalized by  $\frac{1}{2}\rho_p u_i^2$ .

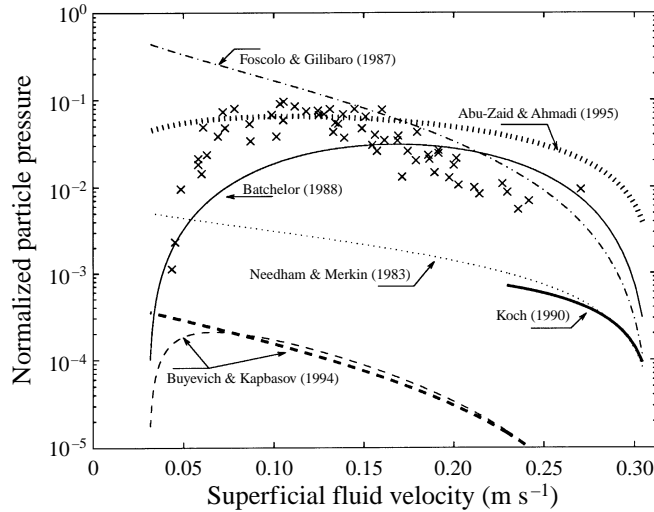


FIGURE 22. Comparison of the experimental results with theoretical models. Experimental results for 3 mm glass particles in a fluidized bed ( $\times$ ). Pressures normalized by  $\frac{1}{2}\rho_p u_i^2$ .

First, this comparison shows that five orders of magnitude are necessary to present the calculated particle pressures from the different models, indicating the poor level of understanding of the phenomena. The qualitative behaviour of the particle pressure for most of these models does not agree with the experimental measurements.

The model closest to the present experimental measurements is the one proposed by Batchelor (equation (1.2)). This prediction works surprisingly well considering that the quadratic dependence on the solid fraction was chosen to fit the two known conditions on solid fraction.

The model proposed by Abu-Zaid & Ahmadi (equation (1.8)) uses the fluid pressure  $P_f$  as a reference. To compare, the reference fluid pressure is taken as  $P_f = \frac{1}{2}\rho_f u_f^2$ ,

where the velocity of the fluid phase  $u_f$  is calculated from the superficial fluid velocity,  $u_o$ , according to  $u_f = u_o/(1 - v)$ . This expression overestimates the value of the particle pressure by a factor of 2 or 3 for low solid fractions ( $v < 20\%$ ), and agrees well with the experimental measurements both in magnitude and slope for intermediate solid fractions ( $25\% < v < 45\%$ ). However, it does not predict a significant decrease in the value of the pressure for concentrations greater than 45%. In their analysis, the particle pressure was considered to be only a fraction of the fluid pressure, which was not known accurately. The approximation given by  $P_f = \frac{1}{2}\rho_f u_f^2$  may not be representative.

To compare with Koch's model (equation (1.5)) the mean velocity of the solid phase,  $u_p$ , was assumed to be zero, and the fluid velocity  $u_f = u_o/(1 - v)$ . Since the model is only for dilute systems, the predicted particle pressure is shown only for  $v < 0.10$ . Strictly speaking the prediction is only valid for  $v < St^{-2/3}$ , which for the 3 mm particle corresponds to  $v < 0.03$ . Accurate measurements could not be obtained at such low concentrations, therefore direct comparison is not possible. However the model appears to agree with the other models at such small solid fractions.

The work of Buyevich & Kapbasov (equation (1.6)) predicts a particle pressure that is considerably smaller than the experimental results. In this work the particle pressure was obtained following a modified kinetic theory. The particles are assumed to be massive enough to ensure that the exchange of momentum and energy is through direct collisions. Using two different expressions to account for the dependence on concentration, they obtain two curves, one which predicts a maximum at a concentration of approximately 50% (thin dashed line) and another that increases monotonically with solid fraction (thick dashed line). Although this approach is collision-based some of the assumptions may not be appropriate, resulting in a poor correspondence with the experiments.

The model of Foscolo *et al.* (equation (1.3)) overestimates the granular pressure but has approximately the same slope as the measurements for solid fractions less than 30%. For all solid fractions the model predicts a monotonic increase of the particle pressure with increasing concentration and does not predict the existence of a maximum particle pressure at an intermediate solid fraction.

## 8. Conclusions

This paper describes experimental measurements of the collisional particle pressure in liquid–solid flows. Defined as the result of particle impacts, the pressure was measured using a high-frequency response transducer that detected individual collisions of particles. The pressure transducer was flush-mounted on the sidewalls of the vertical tube. The time-averaged pressure was calculated from the product of the event rate and the average impulse, which was obtained from hundreds of individual collisions. Results were obtained for a liquid-fluidized bed and for a vertical gravity-driven flow.

In the case of a fluidized bed, the particle pressure shows a clear dependence on the solid fraction. In a concentrated bed the particles cannot move rapidly owing to the geometric limitations of the packed state. This results in low-impulse collisions, leading to a low-particle pressure. On the other hand, for a dilute system, the particles are free to move in the bed but collide with each other and the walls more infrequently. The event rate decreases, resulting in a lower value of the particle pressure. At intermediate concentrations the combination of these two competing mechanisms yields a maximum particle pressure. Similar results were found for all particle diameters and densities; the magnitude of the particle pressure appears to

scale with  $\rho_p u_t^2$ , where  $\rho_p$  and  $u_t$  are the density and the terminal velocity of the particle respectively. However, the results of the normalization show that other parameters might influence the magnitude of the particle pressure. Experiments were performed in two different test sections. The diameter of the test section was found to have little influence on the particle pressure.

The dependence of the particle pressure on the solid fraction in the case of the gravity-driven flow was not as clear as in the case of a fluidized bed. For the same particles the magnitude is approximately the same as in the case of the fluidized bed, but the appearance of a maximum for an intermediate solid fractions is not as evident. Cocurrent and countercurrent flow were both examined but the flow direction did not affect the particle pressure.

The probability density functions were calculated for the maximum collision pressure, collision duration, and collision impulse. In concentrated flows, low-pressure and low-impulse collisions occur more frequently. As the solid fraction decreases the probability of collisions of larger pressures and impulses increases. The analysis of the PDF of the collision duration led to the discovery of two distinct contributions to the particle pressure: one that results from direct collisions of particles with the pressure transducer, and another resulting from collisions between particles in the bulk producing pressure pulses that are transmitted through the interstitial fluid.

A review of the existing models of the particle pressure and a direct comparison with the measurements were also presented. Essential differences were found in the formulation of some of these models. The model proposed by Batchelor (1988) was found to be closest to the experimental results. However, a more quantitatively accurate model remains to be developed.

The authors are grateful to Professor Charles Campbell for helpful discussions and suggestions. The National Council for Science and Technology of Mexico (CONACYT) is acknowledged for partially supporting R. Zenit during his graduate sojourn at the California Institute of Technology.

#### REFERENCES

- ABU-ZAID, S. & AHMADI, G. 1995 A thermodynamically consistent rate-dependent model for turbulent two-phase flows. *Intl J. Non-Linear Mech.*, **30**, 509–529.
- AHMADI, G. 1987 On the mechanics of incompressible multiphase suspensions. *Adv. Water Res.* **10**, 32–43.
- AHMADI, G. & MA, D. 1990 A thermodynamic formulation for dispersed multiphase turbulent flows - I. basic theory. *Intl J. Multiphase Flow* **16**, 323–340.
- AVALONE, E. A. & BAUMEISTER III, T. 1896 *Mark's Standard Handbook for Mechanical Engineers*, 9th edn. McGraw-Hill.
- BATCHELOR, G. K. 1988 A new theory of the instability of a uniform fluidized bed. *J. Fluid Mech.* **193**, 75–110.
- BEN-AMMAR, F., KAVIANY, M. & BARBER, J. R. 1992 Heat transfer during impact. *Intl J Heat Mass Transfer* **35**, 1495–1506.
- BERNIER, R. N. 1982 Unsteady two-phase flow instrumentation and measurement. PhD thesis, California Institute of Technology, Pasadena, California.
- BULTHUIS, H. F., PROSPERETTI, A. & SANGANI, A. S. 1995 'Particle stress' in disperse two-phase potential flow. *J. Fluid Mech.* **294**, 1–16.
- BUYEVICH, Y. A. & KAPBASOV, S. K. 1994 Random fluctuations in a fluidized bed. *Chem Engng Sci.* **49**, 1229–1243.
- CAMPBELL, C. S. 1990 Particle pressures in gas-fluidized beds. *Ann. Rev. Fluid Mech.* **22**, 57–92.
- CAMPBELL, C. S. & WANG, D. G. 1990 Particle pressures in gas-fluidized beds. *J. Fluid Mech.* **227**, 495–508.

- FOSCOLO, P. U., DI FELICE, R. & GIBILARO, L. G. 1989 The pressure field in an unsteady-state fluidized bed. *AICHE J.* **35**, 1921–1926.
- FOSCOLO, P. U. & GIBILARO, L. G. 1987 Fluid dynamic stability of fluidized suspensions. *Chem. Engng Sci.* **39**, 1485–1500.
- GOLDSMITH, W. 1960 *The Theory and Physical Behaviour of Colliding Solids*. London, Edward Arnold Publishers.
- HARRISON, D., DAVIDSON, J. F. & DEKOCK, J. W. 1961 On the nature of aggregative and particulate fluidization. *Trans. Inst. Chem. Engrs* **41**, 13.
- JACKSON, R. 1963 The mechanics of fluidized beds: Part i: the stability of the state of uniform fluidization. *Trans. Inst. Chem. Engrs* **41**, 13–41.
- JACKSON, R. 1985 Hydrodynamic stability of fluid-particle systems. In *Fluidization* (ed. J. Davidson, R. Clift & D. Harrison), 2nd Edn. Academic.
- JIN, C. 1996 Generic stability model and experimental study of liquid-fluidized beds. PhD thesis, University of Southern California, Los Angeles California.
- KOCH, D. L. 1990 Kinetic theory for a monodisperse gas-solid suspension. *Phys. Fluids A* **2**, 1711–1723.
- KYTÖMAA, H. K. & BRENNEN, C. E. 1986 Some observations of flow patterns and statistical properties of three component flows. *Trans. ASME: J. Fluids Engng* **110**, 76–84.
- KUMAR, S., HART, D. P. & BRENNEN, C. E. 1990 Granular pressure measurement in fluidized beds. In *ASME Cavitation and Multiphase Flow Forum, Toronto, Canada*.
- LIU, C.-H., NAGEL, R. H., SCHECTER, D. A., COPPERSMITH, S. N., MUJUMDAR, S., NARAYAN, O. & WITTEN, T. A. 1995 Force fluctuations in bead packs. *Science* **269**, 513–515.
- NEEDHAM, D. J. & MERKIN, J. H. 1983 The propagation of a voidage disturbance in a uniformly fluidized bed. *J. Fluid Mech.* **131**, 427–454.
- NOTT, P. R. & BRADY, J. F. 1994 Pressure-driven flow of suspensions: simulations and theory. *J. Fluid Mech.* **275**, 157–199.
- ROCO, M. C. & ADDIE, G. R. 1987 Erosion wear in slurry pumps and pipes. *Powder Technol.* **50**, 35–46.
- SANGANI, A. S., MO, G., TSAO, H. K. & KOCH, D. L. 1996 Simple shear flows of dense gas-solid suspensions at finite Stokes numbers. *J. Fluid Mech.* **313**, 309–341.
- TSAO, H. K. & KOCH, D. L. 1995 Simple shear flows of dilute gas-solid suspensions. *J. Fluid Mech.* **296**, 211–245.
- WALLIS, G. B. 1969 *One-Dimensional Two Phase Flow*. McGraw-Hill.
- ZENIT, R. 1997 Collisional mechanics in liquid-solid flows. PhD thesis, California Institute of Technology, Pasadena, California.